Journal of Computational Neuroscience 14, 119–138, 2003

Spike-Based Synaptic Plasticity and the Emergence of Direction Selective Simple Cells: Mathematical Analysis*

W. SENN AND N.J. BUCHS
Physiological Institute, University of Bern, Bühlplatz 5, CH-3012 Bern, Switzerland
wsenn@cns.unibe.ch
buchs@cns.unibe.ch

Received February 12, 2002; Revised May 21, 2002; Accepted May 24, 2002

Action Editor: Jonathan D. Victor

Abstract. In the companion paper we presented extended simulations showing that the recently observed spike-timing dependent synaptic plasticity can explain the development of simple cell direction selectivity (DS) when simultaneously modifying the synaptic strength and the degree of synaptic depression. Here we estimate the spatial shift of the simple cell receptive field (RF) induced by the long-term synaptic plasticity, and the temporal phase advance caused by the short-term synaptic depression in response to drifting grating stimuli. The analytical expressions for this spatial shift and temporal phase advance lead to a qualitative reproduction of the frequency tuning curves of non-directional and directional simple cells. In agreement with in vivo recordings, the acquired DS is strongest for test gratings with a temporal frequency around 1–4 Hz. In our model this best frequency is determined by the width of the learning function and the time course of depression, but not by the temporal frequency of the 'training' stimuli. The analysis further reveals the instability of the initially symmetric RF, and formally explains why direction selectivity develops from a non-directional cell in a natural, directionally unbiased stimulation scenario.

Keywords: spike-timing, dependent synaptic plasticity, short-term synaptic depression, direction selectivity, simple cell, phase advance

1. Introduction

One of the basic operations of the primary visual cortex (V1) is the extraction of very local, well-defined features of the retinal image, being fused with other sources of information in higher cortical areas. The local features encompass luminance contrasts, edges, orientations, and directions of motion (Hubel and Wiesel, 1962). A remarkable property of a broad class of V1 neurons, the simple cells, is that they exhibit (almost) linear spatial and temporal summation: the time course of the subthreshold membrane potential in response to two (spatially disjoint) stimuli is the sum of the responses to the individual stimuli (Reid et al., 1987; Shapley, 1996; Carandini et al., 1997). The most prominent deviations from linearity are the saturation of simple cell responses at high contrast (Albrecht et al., 1984) and the cross-orientation suppression (Morrone et al., 1982). It was recently suggested that a single type of nonlinearity, short-term synaptic depression in thalamocortical projections, would be enough to explain these nonlinear response properties (Carandini et al., 2002). This same synaptic mechanism may also produce directional selective simple cells when depressing and non-depressing synapses are properly arranged within the simple cell receptive field (Chance et al., 1998). Here we analytically describe synaptic depression in response to time varying stimuli. The description

*"Spike-Based Synaptic Plasticity and the Emergence of Direction Selective Simple Cells: Simulation Results" appeared in Volume 13, Issue 3.

includes the entire visual pathway from the retinal input through the thalamic relay to the simple cell response.

The main goal is to study the impact of spike-timing dependent plasticity (STDP) at thalamocortical synapses when the simple cell is exposed to moving sine gratings with random velocities and directions. As shown in our companion paper (Buchs and Senn, 2002, referred to as 'simulation paper'), STDP may explain the development of simple cell direction selectivity (DS). When requiring that directional simple cells evolve from non-directional ones, STDP must operate on the degree of synaptic depression (Markram and Tsodyks, 1996; Senn, 2002) as well as on the synaptic strength (see Bi and Poo, 2001, for a review). We analytically describe the effect of STDP on the simple cell response properties, and focus on the symmetry breaking of the simple cell receptive field (RF) induced by the synaptic modifications.

Short-term synaptic depression at thalamocortical afferents was first described by Stratford et al. (1996). Based on such observations, Chance et al. (1998) suggested that thalamocortical synaptic depression could explain different temporal response properties of simple cells, including DS. The relevant feature of synaptic depression in this context is the phase advance of the synaptic response with respect to a sinusoidally modulated stimulus. When combined with a spatially displaced group of non-depressing synapses this phase advance may generate the simple cell DS. Recent support for short-term synaptic depression in the visual pathway comes from cross-orientation suppression experiments in cats (Freeman et al., 2002). STDP in V1, on the other hand, is supported by in vivo experiments on cats in which spatial shifts in RF of V1 cells were induced by rapid sequential flashing of spatially displaced visual stimuli (Yao and Dan, 2001; Fu et al., 2002).

The specific model we consider consists of a layer of on-center lateral geniculate nucleus (LGN) cells receiving input from the retinal ganglion cells and projecting onto a single simple cell in V1. Afferents in the center of the simple cell RF converge through depressing excitatory synapses while those in the surround converge through non-depressing excitatory synapses onto the simple cell (Fig. 1). In the spirit of a minimal

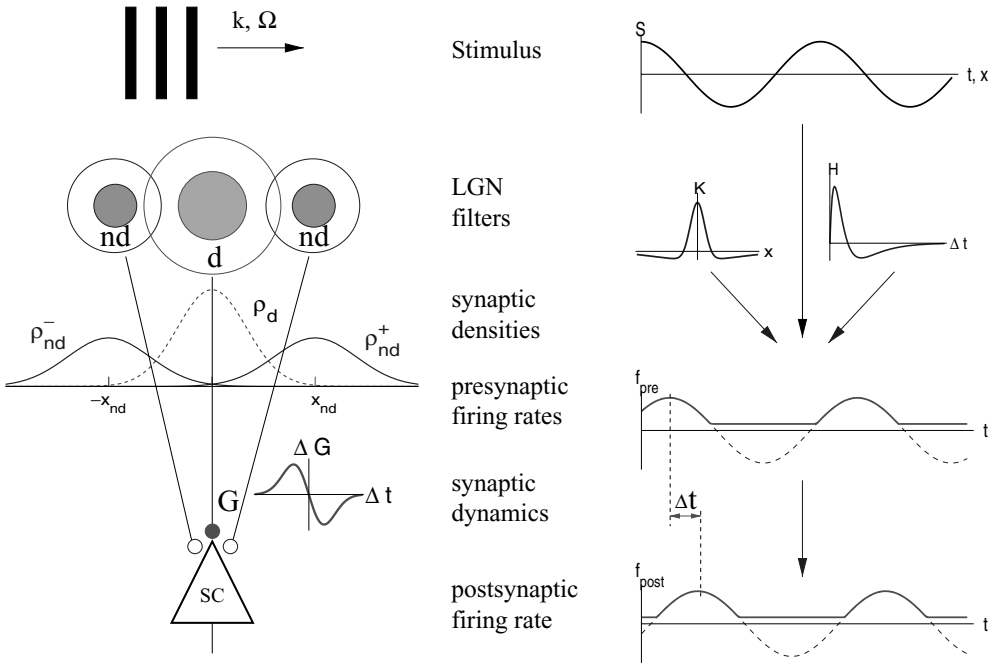

Figure 1. The analytical model. Left: On-center LGN cells project in an initially symmetric arrangement through depressing (d) and non-depressing (nd) synapses onto the simple cell (SC). The total input is determined by fixed synaptic densities from the LGN layer (ρ_d and $\rho^{\pm}_{nd}$), and by the synaptic strengths (G) which are subject to the synaptic modification (ΔG as a function of the pre- and postsynaptic spike time differences). Right: The drifting, sinusoidally modulated grating (S) is processed by a linear spatio-temporal LGN filter (K and H, respectively), followed by a half-rectification (f_{pre}). The timing (Δt) between pre- and postsynaptic spike rates of the simple cell (f_{pre} and f_{post}, respectively) determines whether a synapse is predominantly up- or downregulated. The sketch shows f_{post} as a rectified sine, although the true postsynaptic rate is distorted (see Fig. 2).

model we discard off-center excitatory and inhibitory LGN afferents and, in a first step, we only consider the modification of the absolute synaptic strength of the depressing synapses. To capture the modifications of the simple cell RF we calculate the output frequencies of LGN cells, the degree of synaptic depression, the total postsynaptic current, and the effect of the synaptic long-term modifications. The nonlinearities ascribed to the rectification of the LGN and simple cell responses are thereby neglected. Our analysis yields direct dependencies of the direction selectivity on the stimulus velocity, on the time constant of synaptic depression, and on the width of the synaptic learning window.

The basic mechanism underlying the development of DS is that, in response to drifting light gratings, the temporally asymmetric STDP induces a shift of the depressing RF center opposite to the stimulus direction. This counter directional shift occurs because the synaptic rule strengthens synapses which are activated immediately before the postsynaptic cell fires most, while it weakens those synapses which are activated immediately after. As we show, the spatial shift of the depressing synapses enhances the simple cell response to subsequent gratings moving in the same direction. When stimulated from the other direction however, the two contributions disintegrate because the spatial shift changes its sign, but not the temporal shift (see Fig. 3c). Symmetry breaking is revealed to occur through a positive feedback loop: Any slight RF asymmetry enhances the response to one of the two directions, this further strengthens the synaptic connection which led to the increased response, and the RF symmetry is broken further. This feedback mechanism explains the development of DS even for an unbiased set of stimuli with gratings moving equally often and with different speeds in opposite directions. The paper concludes by showing that the spatio-temporal RF formed by these mechanisms is inseparable. A short form of the present results appeared in Senn (2002).

2. Model and Methods

2.1. *Spatio-Temporal Receptive Field of LGN Cells*

The visual stimuli consist of drifting light gratings specifying the luminance as a function of time t and retinal position x measured in degrees. Neglecting the physical units such a stimulus is given by $S(x,t) = \cos(kx - \Omega t)$, with period $T = \frac{2\pi}{\Omega}$ [ms] and wave length $\lambda = \frac{2\pi}{k}$ [deg]. Each retinal position is associated with an on-center LGN cell whose spatio-temporal receptive field is characterized by a linear filtering followed by a rectification (see Fig. 1). Following Maex and Orban (1996), the instantaneous firing rate of a LGN cell with RF centered at retinal position x is

$$f_{pre}(x,t) = \max\left\{\pm A(C)\int_{-\infty}^{\infty}\int_{-\infty}^{t} d\tilde{t}\, d\tilde{x}\; K(x-\tilde{x}) \times H(t-\tilde{t})S(\tilde{x},\tilde{t}),\, f_{pre}^{back}\right\}, \quad (1)$$

where the spatial filter K is modeled by a difference of Gaussians and the temporal filter H by a difference of a fast and slow alpha-function (Maex and Orban, 1996),

$$K(x) = \frac{1}{\sqrt{2\pi}\sigma_c}\exp\left(-\frac{x^2}{2\sigma_c^2}\right) - \frac{1}{\sqrt{2\pi}\sigma_s}\exp\left(-\frac{x^2}{2\sigma_s^2}\right), \quad \sigma_c < \sigma_s, \quad (2)$$

$$H(t) = \frac{2}{\tau_f^2}t\exp\left(-\frac{t}{\tau_f}\right) - \frac{1}{\tau_s^2}t\exp\left(-\frac{t}{\tau_s}\right), \quad \tau_f < \tau_s. \quad (3)$$

The factor $A(C)$ in (1) scales the LGN cell frequency and depends on the stimulus contrast C as specified in Appendix A.1. On-center and off-center LGN cells are formally distinguished by the choice of the plus and minus, respectively, in (1). The parameters chosen here and in the simulation paper are $\sigma_c = 0.3$ deg, $\sigma_s = 1.5$ deg, $\tau_f = 16$ ms and $\tau_s = 32$ ms.

In the present analysis we restrict ourselves to on-center cells and discard the nonlinear rectification in (1). We therefore assume that the input from the LGN onto the V1 simple cell is specified by a presynaptic spike rate of the form

$$f_{pre}(x,t) = f_{pre}^0 + f_{pre}^1\cos(kx - \Omega t), \quad (4)$$

with average rate f_{pre}^0 and modulation amplitude f_{pre}^1 given by $f_{pre}^0 = f_{pre}^1 = \frac{1}{2}A(C)A_\circ(k,\Omega)$, see Appendix A.1 for explicit expressions and Fig. 4a showing the amplitude f_{pre}^1 as a function of the temporal frequency Ω.

2.2. *Spatio-Temporal Receptive Field of the Simple Cell*

The receptive field of the model V1 cell on the LGN layer is specified by 3 Gaussian clusters of

on-center afferents projecting through depressing and non-depressing synapses onto the simple cell (Fig. 1). The effective synaptic strength (weight) from the LGN layer at position x to the simple cell, $G^{eff}(x)$, is determined by the product of the LGN cell density times the strength of an individual connection at that position, $G^{eff}(x) = \rho(x)G(x)$. In the initial configuration the synaptic weights of the depressing and non-depressing synapses each have the same value, $\bar{G}^{\circ}_{d/nd}$. Assuming Gaussian densities for the centered depressing and the left/right non-depressing clusters, the initial effective strengths become (cf. Figs. 1 and 3c)

$$\bar{G}^{eff,\pm}_{nd}(x) = \rho^{\pm}_{nd}(x)\bar{G}_{nd}(x) = \frac{\bar{G}^{\circ}_{nd}}{\sqrt{2\pi}\sigma_{nd}} \exp\left(-\frac{(x \pm x_{nd})^2}{2\sigma^2_{nd}}\right), \quad (5)$$

$$\bar{G}^{eff}_{d}(x) = \rho_d(x)\bar{G}_d(x) = \frac{\bar{G}^{\circ}_{d}}{\sqrt{2\pi}\sigma_{d}} \exp\left(-\frac{x^2}{2\sigma^2_{d}}\right). \quad (6)$$

2.3. Short-Term Synaptic Dynamics

The model of synaptic transmission considers a limited source of vesicles with some non-negligible recovery time after each synaptic release. In the simulation paper, the stochastic recovery process is assumed to be Poissonian with time constant τ_{rec}. Given a releasable vesicle, this vesicle is discharged with probability P_{dis} upon arrival of a presynaptic spike. The total probability of releasing a vesicle in response to a presynaptic spike is $P_{dis}P_v$, where P_v is the probability of encountering a releasable vesicle. This probability is governed by the equation

$$\frac{dP_v}{dt} = \frac{1 - P_v}{\tau_{rec}} - P_{dis}P_v \sum_{pre} \delta(t - t_{pre}), \quad (7)$$

where the sum is taken over all presynaptic spike times t_{pre}. A synaptic release is assumed to trigger an instantaneous current pulse of strength $\bar{G}_d$, and the expected current pulse induced by a depressing synapse is proportional to $G_d = P_{dis}P_v\bar{G}_d$. In the present paper we only consider the mean behavior of (7) obtained by replacing the sum of delta functions with the presynaptic spike rate f_{pre} given by (4), see Eq. (9) below. Non-depressing synapses are characterized by $P_{dis} = 1$ and $P_v = 1$ at any time.

2.4. Synaptic Modification and Simple Cell Model

Here we consider a reduced scheme of synaptic modification which, in term of spikes, can be expressed by the learning function

$$L(\Delta t) = -\frac{\Delta t}{\sqrt{2\pi}\tau_L} \exp\left(-\frac{\Delta t^2}{2\tau^2_L}\right), \quad (8)$$

where $\Delta t = t^{rel}_{pre} - t^{sp}_{post}$ is the time difference between a presynaptic release and a post-synaptic spike. This function has a maximum and minimum at $-\tau_L$ and τ_L, respectively, determining the positive (long-term potentiation, LTP) and a negative (long-term depression, LTD) term of the learning rule. The strength $\bar{G}_d$ of a depressing synapse is changed proportionally to $L(\Delta t)$. Equation (8) represents a convenient reduction of the full scheme of the synaptic modification based on internal variables tracing the pre- and post-synaptic activities (see simulation paper). In the present mean field analysis (8) enters as a kernel in the convolution of the presynaptic release rate with the postsynaptic spike rate (see Eq. (31) below). Beside the change of the synaptic strength $\bar{G}_d$, we will also consider the modification of the discharge probability P_{dis} according to the same rule (8).

Finally, as a simple cell model we consider a linearized version of the conduction-based integrate-and-fire neuron used in the simulation paper. In particular, we assume a linear frequency-current relationship for the V1 cell. We normalize the synaptic strength such that the total postsynaptic current $I(t)$ can be identified with the instantaneous postsynaptic spike frequency f_{post}.

3. Results

3.1. Temporal Phase Advance of the Synaptic Response from LGN to V1

We first describe the average response of a depressing synapse to a sinusoidally modulated Poisson spike train with instantaneous spike rate $f_{pre}(t) = f^0_{pre} + f^1_{pre}\cos(\Omega t)$. The average release rate is given by $f_{rel}(t) = P_{rel}(t)f_{pre}(t)$ and vesicle release probability is itself a product of the discharge probability, and the probability of a vesicle being recovered, $P_{rel} = P_{dis}P_v$, see Senn et al. (2000). According to (7) the dynamics of the average vesicle probability P_v is determined

by

$$\frac{dP_v}{dt} = \frac{1 - P_v}{\tau_{rec}} - P_{dis} P_v f_{pre}(t), \tag{9}$$

where, for notational conveniences, we discard from writing the expectation value symbols. For stationary presynaptic spike rates $f_{pre}(t) = f^0_{pre}$ one may rewrite this differential equation in the form $\frac{dP_v}{dt} = \frac{P^{ss}_v - P_v}{\tau^{ss}_{rec}}$ with a (expected) steady state vesicle probability

$$P^{ss}_v = \frac{1}{1 + \tau_{rec} P_{dis} f^0_{pre}} \tag{10}$$

and an effective time constant

$$\tau^{ss}_{rec} = \frac{\tau_{rec}}{1 + \tau_{rec} P_{dis} f^0_{pre}}. \tag{11}$$

The dynamics of the vesicle probability $P_v(t)$ in response to the sine wave stimulation (4) can be approximated by the zeroth- and first-order Fourier components (Fig. 2b),

$$P_v(t) \approx P^0_v + P^1_v \cos(\Omega t + \phi). \tag{12}$$

The Fourier coefficients and the phase advance depend on the modulation frequency according to (see Appendix A.2)

$$P^0_v \approx P^{ss}_v \frac{2F^2}{2F^2 - \left(P_{dis} f^1_{pre}\right)^2}, \tag{13}$$

$$P^1_v \approx P^0_v \frac{P_{dis} f^1_{pre}}{F}, \tag{14}$$

$$\phi \approx \pi - \arctan\left(\tau^{ss}_{rec}\Omega\right), \tag{15}$$

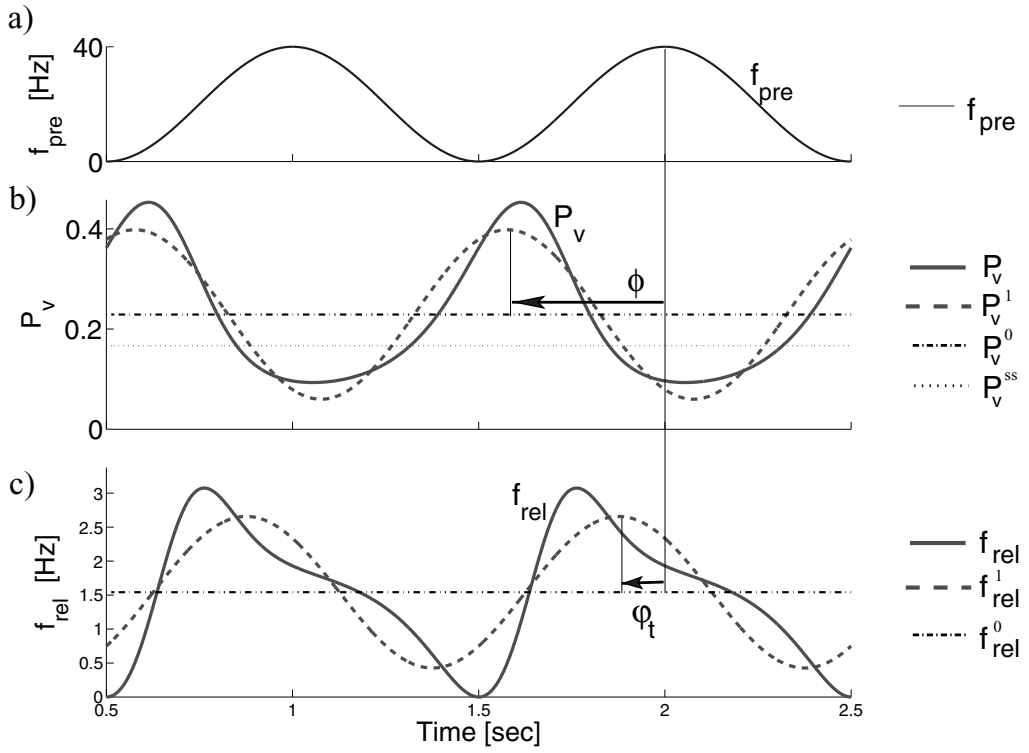

Figure 2. Synaptic depression and its first Fourier approximation. **a:** Presynaptic firing rate $f_{pre}(t)$. **b:** Time course of the vesicle probability P_v obtained by integrating Eq. (9) (full line) and the first Fourier approximation specified by Eqs. (12)–(15) (thick dashed line). The zeroth Fourier component (dashed-dotted horizontal line, Eq. (13)) is markedly higher than the steady state for the same mean frequency f^0_{pre} (thin dotted horizontal line, Eq. (10)). The arrow shows the phase advance ϕ, Eq. (15), of the $P_v(t)$ with respect to the presynaptic firing rate shown in (a). **c:** Time course of the synaptic release rate $f_{rel} = P_{dis} P_v f_{pre}$ when using the exact form for $P_v(t)$ (full line, Eq. (16)) and its first order Fourier approximation (dashed sinewave, Eqs. (18)–(21)). The zeroth Fourier component, Eq. (19), is represented as a dashed-dotted line. The arrow shows the phase advance φ_t, Eq. (21), of (the first order Fourier approximation of) the release rate with respect to the presynaptic spike rate shown in (a). For parameter values see caption to Fig. 3. Note that the phase advance is roughly a tenth of a cycle (corresponding to the value at the dot in Fig. 4a).

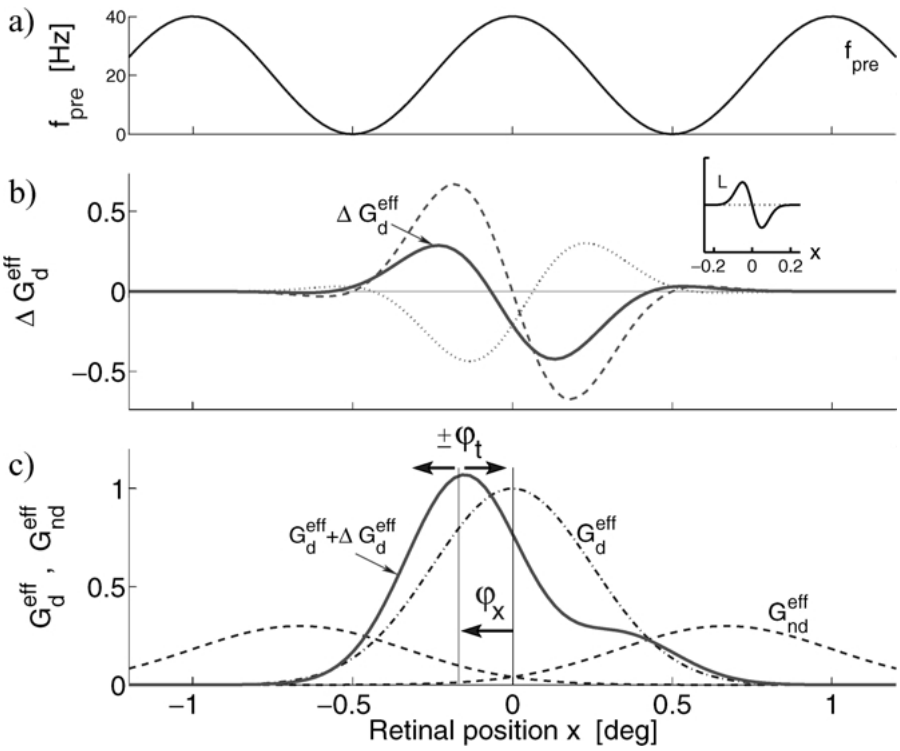

Figure 3. The modification of the effective synaptic strength. **a:** The LGN firing rate f_{pre}, Eq. (4), for a snapshot at time $t = 0$ when the postsynaptic response is largest. **b:** The change of $\Delta\bar{G}_d^{eff}$ according to Eq. (38) (full line) induced by the sinusoidally modulated LGN firing rate in (a). The weight change is composed of two terms originating from depressing synapses (dashed line, first term in Eq. (32)) and non-depressing synapses (dotted line, second term in Eq. (32)). The inset depicts the learning function $L(\frac{kx}{\Omega})$, Eq. (8), as a function of x. Note that the width of the synaptic change reflects the width of the stimulus, and not of the learning function (unless the stimulus is a narrow bar as in Eq. (40)). **c:** The distribution of the effective synaptic strengths in the initial state for the depressing center (dashed-dotted line, $\bar{G}_d^{eff}$) and the non-depressing surround (dashed lines, $\bar{G}_{nd}^{eff}$, cf. Eqs. (5) and (6)). After repeated stimulation with rightwards drifting gratings the effective synaptic strength of the RF center moved to the left (full line, $\bar{G}_d^{eff}(x) + \Delta\bar{G}_d^{eff}(x)$, Eq. (38)). The lower leftwards arrow shows the estimated spatial shift $\varphi_x/k(=-x_{\Delta w}^{peak})$ of the RF center (Eq. (39)). The adjacent left/right arrows on top show the temporal shift of the postsynaptic response from the depressing center expressed in spatial coordinates, $\pm\varphi_t/k$, for a stimulus moving right-/leftwards, cf. Eqs. (21) and (41). For the rightward (preferred) direction the spatial and temporal phase shifts add to a total shift of -0.3 deg (head of top leftwards arrow) while for the leftward (non-preferred) direction they cancel (head of top rightwards arrow). In all the Figs. 2–6 we used the parameter values $\tau_{rec} = 0.5$ s, $P_{dis} = 0.5$ and $f_{pre}^0 = f_{pre}^1 = 20$ Hz, $\tau_L = 50$ ms, $\frac{\Omega}{2\pi} = 1$ Hz, $\frac{k}{2\pi} = 1$ cycle/deg (yielding a spatial wave length $\lambda = \frac{2\pi}{k} = 1$ deg), $x_{nd} = \frac{2}{3}\lambda$, $\sigma_{nd} = \frac{1}{3}\lambda$, $\sigma_4 = \frac{1}{4}\lambda$, $\bar{G}_{nd}^{\circ} = 0.3$, $\bar{G}_d^{\circ} = 1$.

with $F^2 = \Omega^2 + (1/\tau_{rec} + P_{dis} f_{pre}^0)^2$. Note that the average vesicle probability P_v^0 is larger than the steady state P_v^{ss} for the stationary frequency f_{pre}^0 (compare Eqs. (10) and (13)). Figure 2b shows that, in fact, a sinusoidal modulation of the presynaptic spike rate around a constant mean can increase the average synaptic response by almost 50%, just because the dynamics of depression and recovery are not symmetric around the steady state. Note further that for $\Omega \to \infty$, through the dependency $F^2(\Omega)$, the first Fourier component P_v^1 approaches 0, while the zeroth component P_v^0 approaches P_v^{ss}. The phase advance ϕ decreases with $\Omega \to \infty$ from π to $\pi/2$, and, as a function of f_{pre}^0, it monotonically increases with upper bound π. Figure 2b gives an example of the time course of P_v, Eq. (9), and its first Fourier approximation specified by (12)–(15).

We next approximate the instantaneous vesicle release rate $f_{rel} = P_{rel} f_{pre}$. According to (12) we get

$$f_{rel}(t) = P_{rel} f_{pre}(t) = P_{dis} P_v(t) f_{pre}(t) \qquad (16)$$

$$\approx P_{dis}\big(P_v^0 + P_v^1 \cos(\Omega t + \phi)\big) \times \big(f_{pre}^0 + f_{pre}^1 \cos \Omega t\big). \qquad (17)$$

A measure of the phase advance of the release rate with respect to presynaptic firing rate is obtained by

calculating the first Fourier approximation of (17),

$$f_{rel}(t) \approx f^0_{rel} + f^1_{rel}\cos(\Omega t + \varphi_t) \tag{18}$$

where the zeroth and first Fourier coefficients and the temporal phase advance are themselves approximated by (cf. Appendix A.2)

$$f^0_{rel} \approx P_{dis}P^0_v f^0_{pre} - P_{dis}P^1_v f^1_{pre}\frac{1}{2\tau^{ss}_{rec}F}, \tag{19}$$

$$f^1_{rel} \approx P_{dis}P^0_v f^1_{pre}\frac{\sqrt{\Omega^2+\tau^{-2}_{rec}}}{F}, \tag{20}$$

$$\varphi_t \approx \arctan\left(\frac{P_{dis}f^0_{pre}\tau^2_{rec}\Omega}{1+P_{dis}f^0_{pre}\tau_{rec}+\tau^2_{rec}\Omega^2}\right). \tag{21}$$

The first Fourier component f^1_{rel} as a function of the temporal frequency $\Omega/(2\pi)$ is depicted in Fig. 4a.

As an example, the exact solution of f_{rel}, obtained by integrating Eq. (9), is shown in Fig. 2c, together with the first Fourier approximation (18)–(21). According to (21), the temporal phase advance tends to zero for very slow and very fast modulation frequencies, $\varphi_t \to 0$ for $\Omega \to 0$ and $\Omega \to \infty$, since Ω arises in the numerator of (21) and F^2 scales with Ω^2, respectively. In addition, expression (21) allows us to estimate the temporal stimulus frequency leading to a maximal phase advance φ_t,

$$\Omega_{\varphi_t max} \approx \frac{1}{\tau_{rec}}\sqrt{1+P_{dis}f^0_{pre}\tau_{rec}}. \tag{22}$$

With an average LGN frequency of $f^0_{pre} = 40$ Hz, a vesicle recovery time constant of $\tau_{rec} = 0.5$ s and a discharge probability of $P_{dis} = 0.5$, a maximal phase advance is reached according to (22) for a stimulus frequency of $\Omega/(2\pi) \approx 1.0$ Hz (dot in Fig. 4a).

We tested the above approximations for various physiologically relevant parameter values and in general found good matches with simulations using unrectified sinusoidal LGN spike rates (as in Eq. (4)). However, when compared with simulations using rectified LGN rates, the first Fourier component and the phase shifts were underestimated. This is because in the rectification period the synapses recovered more than they would for an unrectified sinusoidal modulation of the LGN firing rate (see Fig. 1, right). When applied to individual synaptic responses the above approximations

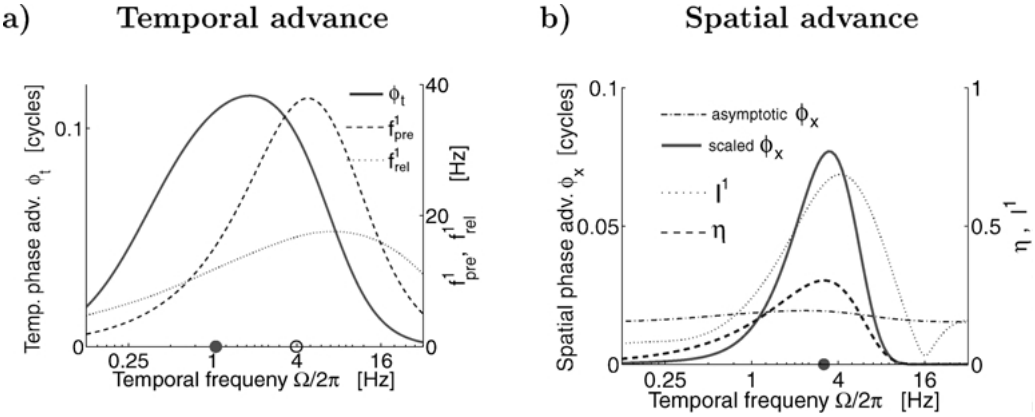

Figure 4. Analytical results: temporal tuning curves. **a:** The modulation amplitude of the LGN frequencies ($f^1_{pre} = \frac{1}{2}A(C)A_\circ(k,\Omega)$, dashed line, Eq. (4), using the analytical expressions in A.1), the first Fourier component of the synaptic release rate (f^1_{rel}, dotted line, Eq. (20), scaled up by a factor of 10), and the temporal phase advance of the release rate with respect to the presynaptic spike rate (φ_t, thick line, Eq. (21)), as a function of the temporal frequency of the drifting grating. Dot on abscissa: estimated location of the maximal phase advance, Eq. (22). The temporal phase advance at 1 Hz is roughly a tenth of a cycle ($\varphi \approx 0.1$) and corresponds to the one in Fig. 2c. Circle on abscissa: estimated location of the maximal LGN modulation amplitude, Eq. (24). Note that synaptic depression acts as a high pass filter (the peak of f^1_{rel} is right from the peak of f^1_{pre}). **b:** The spatial phase shift of the effective synaptic strength induced by the learning rule (φ_x, Eq. (39)), scaled by the 'speed of convergence', i.e. by the factor $f^1_{rel}I^1\eta(\Omega)/\tau_L$ in Eq. (38) (thick line). This scaled phase shift gives an estimate of the effective RF shift reached after stimulating for a fixed time with a unidirectionally moving grating of frequency Ω. Superposed is the factor $\eta(\Omega)$ (dashed line, Eq. (34)) representing the Fourier transform of the learning function, I^1 (dotted line, Eq. (36)) reflecting the postsynaptic current, and the asymptotic phase shift (dashed-dotted line, Eq. (39)) which is almost independent of Ω. The dot on the abscissa represents the estimated location of the maximal phase shift, Eq. (37). The shape of the phase shift curves in (a) and (b) are similar to those obtained for the large scale simulations (Fig. 5 of the simulation paper). In the simulations, however, the phase shifts are roughly three times smaller due to the spatial averaging of the nonlinear synaptic responses performed by the simple cell.

are therefore only good if the rectification does not cut off the LGN response over a too long period (which is the case if the F0 component of the LGN firing rate is larger than the F1 component). This caution, however, is only necessary if the above formulas are used as an estimate of the individual synaptic response. When applied to the total response of the full population of depressing synapses, we always found reasonable results (as shown by a comparison between Fig. 4 and Fig. 5 in the simulation paper), even if the LGN response is rectified during half a cycle. The good match in this case comes from the fact that the nonlinearities are averaged out by the different temporal offsets of the individual responses, but also by the push-pull mechanism which "linearizes" the overall LGN response.

3.2. *Stimulus-Induced Responses of LGN and V1 Cells*

The firing rates of the LGN cells, as defined by the spatio-temporal filtering and the sub-sequent half-rectification in (1), strongly depend on the spatial and temporal frequencies of the stimulus. Evaluating the double integral in (1) yields a temporally shifted moving sinewave with amplitude $A(C)A_\circ(k, \Omega)$ specified in Appendix A.1 (see also Fig. 4a, dashed line). According to this expression the LGN frequencies decay towards background frequency, $f_{pre} \to f_{pre}^{back}$, if either the spatial or temporal stimulus frequencies tend to infinity ($k, \Omega \to \infty$), or if the spatial stimulus frequency tends to zero ($k \to 0$), cf. Eq. (50). The LGN frequencies also decrease (although not to the background frequency) if the temporal stimulus modulation becomes slow ($\Omega \to 0$). The analytical expressions in Appendix A.1 also allow us to estimate the spatial and temporal stimulus frequencies yielding the maximal LGN spike rates,

$$k \approx \frac{2}{\sigma_c}\sqrt{\frac{\ln r_\sigma}{r_\sigma^2 - 1}}, \quad \text{with } r_\sigma = \sigma_s/\sigma_c, \tag{23}$$

$$\Omega \approx \frac{1}{\tau_f}\sqrt{\frac{1 - r_\tau^{-1/2}}{r_\tau^{3/2} - 1}}, \quad \text{with } r_\tau = \tau_s/\tau_f. \tag{24}$$

With the standard choice of parameters (see Section 2.1) we get a maximal LGN firing rate for a spatial stimulus frequency of $k/(2\pi) \approx 0.3$ cycles/deg, and a temporal stimulus frequency of $\Omega/(2\pi) \approx 4.0$ Hz (circle in Fig. 4a). These estimates closely match the peaks of the LGN cell tuning curves (Saul and Humphrey, 1990) as well as the simple cell tuning curves (Saul and Humphrey, 1992, see also Fig. 6b).

We next calculate the response of our model simple cell to a drifting grating. In our reduced neuron model this amounts to summing up the different synaptic currents over the simple cell RF. Neglecting the ionic driving forces, the currents induced by the non-depressing and depressing currents, respectively, are

$$I_{nd}^{\pm}(t) = \int_{-\infty}^{\infty} dx\, \bar{G}_{nd}^{eff,\pm}(x) f_{pre}(x, t), \tag{25}$$

$$I_d(t) = \int_{-\infty}^{\infty} dx\, \bar{G}_d^{eff}(x) f_{rel}(x, t). \tag{26}$$

The presynaptic spike rate f_{pre} (which for non-depressing synapses is equal to f_{rel}) is given by Eq. (4), while the presynaptic release rate f_{rel} for depressing synapses (characterized by $\tau_{rec} > 0$) takes the form

$$f_{rel}(x, t) \approx f_{rel}^0 + f_{rel}^1 \cos(kx - \Omega t - \varphi_t) \tag{27}$$

with phase shift and Fourier coefficients given by (21) and (20). Inserting the effective synaptic strengths (5) and (6) into the above integrals, one obtains the currents

$$I_{nd}^{\pm}(t) = \bar{G}_{nd}^{\circ}\big(f_{pre}^0 + s_{nd} f_{pre}^1 \cos(\pm k x_{nd} - \Omega t)\big), \tag{28}$$

$$I_d(t) = \bar{G}_d^{\circ}\big(f_{rel}^0 + s_d f_{rel}^1 \cos(\Omega t + \varphi_t)\big), \tag{29}$$

with factors $s_{d/nd} = \exp(-(\sigma_{d/nd} k)^2/2)$ for the modulation amplitude of the synaptic responses (see Appendix A.3). The total synaptic current flowing into the V1 cell is the sum of the currents induced by the left and right non-depressing surround and the depressing center,

$$I(t) = I_{nd}^{-}(t) + I_{nd}^{+}(t) + I_d(t). \tag{30}$$

According to our simplified simple cell model the postsynaptic spike frequency is proportional to the total postsynaptic current (30) and this also drives the synaptic modification.

3.3. *Stimulus-Induced Spatial Shift of the Simple Cell RF*

In a next step we estimate the induced change in the synaptic connections projecting onto the simple cell. To simplify matters we assume a fixed discharge probability P_{dis} for all connections, and only modify the strength $\bar{G}_d$ of the depressing synapses. According to

the learning rule (8), the change of the synaptic strength over a full cycle of the grating is

$$\Delta\bar{G}_d(x) = \frac{1}{T}\int_0^T dt \int_{-\infty}^{\infty} d\tilde{t} L(\tilde{t}-t) f_{rel}(x,\tilde{t}) I(t), \tag{31}$$

where $T = \frac{2\pi}{\Omega}$ is the cycle period, I the total postsynaptic current given by (28)–(30), and f_{rel} the presynaptic release rate of the depressing synapses induced by a rightwards moving grating (Eq. (27)). Evaluating the double integral (see Appendix A.3), the change in the synaptic strength linked to the retinal position x becomes

$$\begin{aligned}\Delta\bar{G}_d(x) &= -\frac{1}{2}\eta(\Omega)\left[I_d^1 \sin(kx) - I_{nd}^1 \sin(kx-\varphi_t)\right] &(32)\\ &= -\frac{1}{2} f_{rel}^1 I^1 \eta(\Omega)\sin(kx+\gamma), &(33)\end{aligned}$$

with normalization factor $\eta(\Omega)$ and coefficients I_d^1, I_{nd}^1, I^1 and γ given by

$$\begin{aligned}\eta(\Omega) &= \tau_L^2 \Omega \exp\left(-\tau_L^2\Omega^2/2\right), &(34)\\ I_d^1 &= s_d \bar{G}_d^{\circ} f_{rel}^1, \\ I_{nd}^1 &= -2 s_{nd} \bar{G}_{nd}^{\circ} f_{pre}^1 \cos(kx_{nd}), &(35)\\ I^1 &= \sqrt{\left(I_d^1\right)^2 + \left(I_{nd}^1\right)^2 - 2 I_d^1 I_{nd}^1 \cos\varphi_t}, &(36)\\ \tan\gamma &= \frac{I_{nd}^1 \sin\varphi_t}{I_d^1 - I_{nd}^1\cos\varphi_t}.\end{aligned}$$

Note that, up to a scaling factor, $\eta(\Omega)$ represents the Fourier transform of the learning function $L(\Delta t)$, while I^1 represents the modulation amplitude of the postsynaptic current (cf. Eqs. (42) and (43) below). Hence, the strength (or 'speed') of the synaptic change is roughly proportional to the product of the presynaptic release rate, the postsynaptic current, and the Fourier transform of the learning function. We have chosen the synaptic strengths and the spatial frequency such that roughly $I_d^1 \approx I_{nd}^1$, i.e., such that the postsynaptic currents induced by the depressing and non-depressing synapses, respectively, contribute to a similar extent to the synaptic modification (note that for the present choice of parameter values we have $kx_{nd} = 4\pi/3$ and, according to Eq. (35), I_{nd}^1 is positive; in turn, for $kx_{nd} = \pi/2$, or $\lambda = 4x_{nd}$, I_{nd}^1 would vanish). In fact, the form of the factor I^1 (Eq. (36)) shows that the change of the synaptic strength, $\Delta\bar{G}_d$, is maximal if I_d^1 and I_{nd}^1 are of the same size (cf. Fig. 5). While depressing and non-depressing synapses work together in generating DS (in the sense of a temporal overlap) the two populations partly interfere during the learning process. This is because in an initial phase the postsynaptic current originating from the depressing and non-depressing synapses are phase shifted by roughly half a cycle and therefore have opposite effects on the synaptic change (see the two terms in Eq. (32) and the dashed and dotted lines in Fig. 3b). Nevertheless, up to the phase shift γ quantifying the interference between the two populations, the overall synaptic change is an anti-symmetric function of space, $\sin(kx)$, and reflects the derivative of the stimulus at the moment when it is aligned with the RF center (see Eq. (33) and Fig. 3b, thick line).

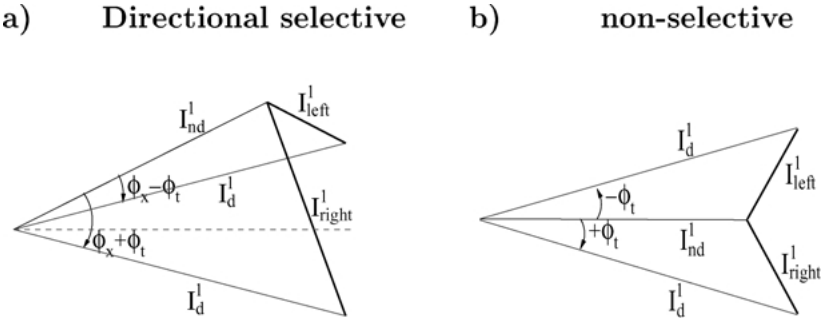

Figure 5. Geometric summation of the two classes of synaptic currents. **a:** The synaptic current from the depressing synapses, I_d^1 (see Eq. (35)), adds by a certain angle with the synaptic current of the non-depressing synapses, I_{nd}^d, to form a third side of a triangle, $I_{left/right}^1$. This side represents the modulation amplitude of the simple cell response for a left- (non-preferred) and rightward (preferred) stimulus direction (cf. Eq. (43)). The size of the response is determined by the angle between the two legs I_d^1 and I_{nd}^1. This angle is given by either the sum or the difference of the spatial and temporal phase shift φ_x and φ_t, respectively (Eqs. (39) and (21)). **b:** If during strobe rearing the motion information is lost, no coherent spatial shift can develop, $\varphi_x = 0$, but P_{dis} may still increase and cause a temporal phase advance φ_t. In this case we have $I_{right}^1 = I_{left}^1$ and the simple cell remains non-directional (see Fig. 9a and c in the simulation paper).

Interestingly, the shape of the weight change $\Delta\bar{G}_d(x)$, Eq. (33), does not depend on the width τ_L of the learning function and depends only weakly (through γ) on the temporal frequency Ω of the grating. Instead, the two parameters only affect the synaptic change through the scaling factor $\eta(\Omega)$ in (33). The interpretation is that for grating stimuli moving repeatedly in one direction (here rightwards) the asymptotic distribution of the synaptic strength is independent of τ_L and Ω, and these parameters do only affect the speed of convergence. According to the dominant factor $\eta(\Omega)$, learning is fastest if the temporal frequency is inversely related to the width of the learning window,

$$\Omega_{\varphi_x max} = 1/\tau_L. \tag{37}$$

For $\tau_L = 50$ ms this yields a maximal speed of convergence at a temporal frequency $\Omega/(2\pi) \approx 3.2$ Hz (dot in Fig. 4b). In a more realistic environment with stimuli moving in different directions the interpretation of (33) is slightly different, because the asymptotic steady state of the unidirectional stimulus scenario is never reached. Rather, due to the counterbalancing effect of the randomly reversing stimulus directions the final synaptic strength becomes proportional to the change $\Delta\bar{G}_d(x)$ itself. As a consequence, the shift in the RF induced by (33) is roughly proportional to the speed of convergence, i.e. to the scaling factors $f^1_{rel} I^1 \eta(\Omega)$. This is confirmed when comparing Fig. 4b, reflecting roughly the function $\eta(\Omega)$, with Fig. 5b in the simulation paper, showing the corresponding spatial phase shift for the large scale simulations.

To make the above statement more quantitative we estimate the shift of the effective synaptic strength $\bar{G}^{eff}_d$ induced by (33). Since the synaptic density is fixed we obtain from (6) a change of the effective synaptic strength of the form

$$\begin{aligned}\Delta\bar{G}^{eff}_d(x) &= \rho_d(x)\Delta\bar{G}_d(x) \\ &= -\frac{1}{2} f^1_{rel} I^1 \eta(\Omega)\rho_d(x)\sin(kx+\gamma),\end{aligned} \tag{38}$$

see Fig. 3b. The maximal change of $\bar{G}^{eff}_d$ is reached at some location $x^{peak}_{\Delta G} < 0$ left of the RF center, i.e. opposite to the stimulus direction. As a rough approximation the asymptotic shift of the RF center in the unidirectional stimulation scenario can be identified by $x^{peak}_{\Delta G}$, although this represents only an upper bound. An estimate of $x^{peak}_{\Delta G}$ based on (38) is given in Appendix A.3. For a drifting grating with spatial frequency $k/(2\pi)$ an upper bound of the (asymptotic) spatial phase shift is

$$\varphi_x = -k x^{peak}_{\Delta G} \approx \frac{k^2\sigma_d\left(\frac{\pi}{2}-\gamma\right)}{1+k^2\sigma_d}. \tag{39}$$

Figure 3c gives an example of the effective synaptic strength, $\bar{G}^{eff}_d(x)$ and its modification according to (38), $\bar{G}^{eff}_d(x) + \Delta\bar{G}^{eff}_d(x)$. It also shows that the Eq. (39) gives a good estimate of the location of the maximal effective weight change, and hence of the RF phase shift.

The explicit formula for φ_x shows that the induced spatial phase shift mainly depends on the width of the stimulus relative to the width of the RF center, $k^2\sigma_d$. For wide gratings, $k \to 0$, the spatial shift tends to zero, $\varphi_x \to 0$, as it should, when the spatial structure in the stimulus disappears. For narrow gratings, $k \to \infty$, the shift converges to the upper bound $\frac{\pi}{2}$, although the interference with the RF surround increases (expressed in the term $\cos(kx_{nd})$ entering through γ, see Eqs. (35) and (36)). For our parameters we have roughly $\gamma \approx 0$, $k^2\sigma_d \approx 1$, and the spatial phase advance becomes $\varphi_x \approx \frac{\pi}{4}$, see Fig. 3b. As noted above, φ_x reflects the asymptotic phase shift reached when stimulating for an infinite time with a rightwards drifting grating. The effective phase shift in a unbiased stimulation scenario depends on the speed of convergence and is obtained by scaling φ_x with the factor $f^1_{rel} I^1 \eta(\Omega)/\tau_L$ obtained from (33), see Fig. 4b. Similarly to the change of the synaptic strength, the effective spatial shift is roughly proportional to the product of the presynaptic release rate, f^1_{rel}, the postsynaptic current, I^1, and the Fourier transform of the learning function, $\eta(\Omega)$.

The fact that the shape of the synaptic change ($\Delta\bar{G}_d(x)$, see Eq. (33)) does not depend on the width of the learning function τ_L, arises from the spatial extension of the stimulus. This is different for a narrow light bar moving with velocity v across the visual field. For such a stimulus the release rate from a depressing synapse is $f_{rel}(x,t) = P_{dis} f^0_{pre}\delta(x - vt)$, and the postsynaptic current from the depressing synapses is $I_d(t) = P_{dis} f^0_{pre}\bar{G}^{eff}_d(vt)$. The synaptic changes induced by this particular current is

$$\begin{aligned}\Delta\bar{G}_d(x) &= \int_{-\infty}^{\infty} dt \int_{-\infty}^{\infty} d\tilde{t} L(\tilde{t}-t) f_{rel}(x,\tilde{t}) I_d(t) \\ &= -c_d x v \exp\left(\frac{-x^2}{2\left((v\tau_L)^2+\sigma_d^2\right)}\right),\end{aligned} \tag{40}$$

with a constant c_d deduced in Appendix A.3, Eq. (59). Thus, in contrast to the sinewave grating stimulus (see

Eq. 33), the synaptic change for an infinitely narrow light bar moving across the RF reflects the shape of the learning function $L(\Delta t)$, Eq. (8), and the spatial width of the change is given by $\sqrt{(v\tau_L)^2 + \sigma_d^2}$. Thus, unlike to the drifting grating scenario where the spatial shift is maximal for stimulus velocities reflecting the width of the learning window (Fig. 4b), the spatial shift monotonically increases with the bar velocity and is only limited by the RF size.

3.4. *Direction Selectivity of Simple Cells After Repeated Stimulations*

We next test whether the synaptic modifications induced by repeated stimulations with a rightwards drifting grating make our model V1 cell selective for this direction. To this end we compare the postsynaptic response to gratings moving in opposite directions after inducing the synaptic modifications. The total current from depressing synapses induced by the right/leftwards moving grating is still given by (29), except that now there is a spatial phase shift φ_x of the synaptic weight distribution $\bar{G}_d(x)$,

$$I^d_{right/left}(t) = \bar{G}^\circ_d\big(f^0_{rel} + s_d f^1_{rel}\cos(\Omega t + \varphi_t \pm \varphi_x)\big), \tag{41}$$

where the '+' corresponds to the right and the '−' to the leftward direction. Beside the temporal phase advance φ_x induced by the short-term synaptic depression, the postsynaptic response is additionally advanced or delayed by a spatial phase φ_x, depending on whether the stimulus moves right- or leftwards. For the 'learned' (rightward) direction, the two phase shifts add, while for the reversed (leftwards) direction they cancel (see arrows in Fig. 3c). The total postsynaptic current for the two stimulus directions, $I_{right/left}$, can be calculated from (28) and (41) using the summation theorem for cosines (see Eq. (53)),

$$\begin{aligned} I_{right/left}(t) &= I^-_{nd}(t) + I^+_{nd}(t) + I^d_{right/left}(t) \\ &= I^0 + I^1_{right/left}\cos(\Omega t + \delta_{right/left}), \end{aligned} \tag{42}$$

with mean current $I^0 = 2\bar{G}^\circ_{nd} f^0_{pre} + \bar{G}^\circ_d f^0_{rel}$, phase shift $\tan\delta_{right/left} = I^1_d \sin(\varphi_t \pm \varphi_x)/(I^1_d \cos(\varphi_t \pm \varphi_x) - I^1_{nd})$, and variables I^1_d, I^1_{nd} given by (35). The amplitude of the current modulation for the left- and rightward stimulus direction is

$$I^1_{right/left} = \sqrt{\big(I^1_d\big)^2 + \big(I^1_{nd}\big)^2 - 2I^1_d I^1_{nd}\cos(\varphi_t \pm \varphi_x)}, \tag{43}$$

with the $+/-$ corresponding to the right/leftward direction, respectively, and with temporal and spatial phase advance given by (21) and (39).

The estimate of the current amplitudes, Eq. (43), has an intuitive geometrical interpretation. If the contribution of the depressing center, I^1_d, and the non-depressing surround, I^1_{nd} (Eq. (35)), are interpreted as side lengths of a triangle with inner angle $\varphi_t \pm \varphi_x$, the length of the third side represents the current amplitude $I^1_{right/left}$ (Fig. 5a). For a leftward moving stimulus the shifts roughly cancel, $\varphi_t - \varphi_x \approx 0$, and the current amplitude is minimal, $I^1_{left} \approx |I^1_d - I^1_{nd}|$. For a stimulus moving in the preferred direction, however, the shifts add towards $\varphi_t + \varphi_x \approx \frac{\pi}{2}$, and the current amplitude in this direction comes closer to $I^1_{right} \approx \sqrt{(I^1_d)^2 + (I^1_{nd})^2}$. The specific form of the coefficient I^1_{nd} also shows that the distance of the non-depressing surround from the RF center, x_{nd}, should roughly correspond to half the stimulus wave length. Without spatial symmetry breaking, a situation which might appear during strobe rearing (see simulation paper, Fig. 9), the simple cell remains undirectional, although the temporal phase advance may be present (Fig. 5b).

As an example Fig. 6a shows the total postsynaptic current according to (42) and (43) for a left- and rightwards drifting grating before (i.e. with $\phi_x = 0$) and after 'training'. The current amplitudes as a function of the temporal frequency of the stimulus is reproduced in Fig. 6b. In agreement with the single cell recordings, and also our large scale simulations, the simple cell is mostly direction selective around 1–4 Hz. It is non-selective for frequencies larger than 8 Hz and smaller than 0.25 Hz. Unlike real simple cells which may still be direction selective at low temporal frequencies, DS in our model is lost due to the relatively fast time course of synaptic depression (see e.g. Fig. 7 b2 in the simulation paper). The loss of DS at high frequencies, however, does well match the simple cell properties. In our model the shape of the DS tuning curve in Fig. 6b essentially reflects the bland-pass properties of synaptic depression (cf. Fig. 4a), and the loss of DS at high frequencies comes from the saturation term (the second term in Eq. (9)), causing the temporal phase shift to vanish for large Ω (see Eq. (21)). Since simple cells act

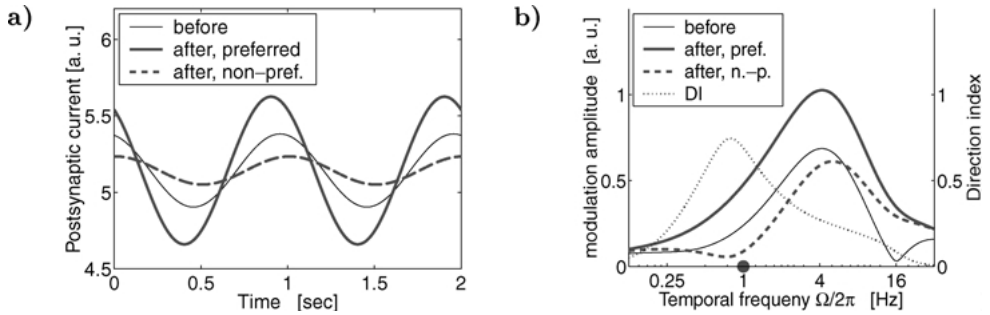

Figure 6. Analytically estimated response of the model simple cell. **a:** Before learning the current response to the left- and rightward drifting grating is the same (thin line, Eq. (30), $\varphi_x = 0$). After 'training' the response from the shifted receptive field center adds with the response from the surround for a stimulus moving in the training direction (thick line, total phase advance with respect to the dashed line: $\varphi_t + \varphi_x \approx \frac{\pi}{2}$) while they fall apart for the reversed direction (dashed line, $\varphi_t + \varphi_x \approx 0$), Eq. (42). **b:** The first harmonics of the response before (thin line, Eq. (36), same response from left and right) and after 'training' (thick line: response to training direction, I^1_{right}; dashed line: response to opposite direction, I^1_{left}, Eq. (43)) as a function of the temporal frequency of the drifting grating (ϕ_t and ϕ_x were evaluated according to 21 and 39, respectively). The training frequency was fixed to $\Omega/(2\pi) = 4$ Hz. The modulation amplitudes of the example in (a) correspond to the values at 1 Hz (dot on abscissa). Since at 1 Hz the temporal phase advance induced by synaptic depression is largest (Fig. 4a and Eq. (22)), the direction index (DI, dotted line, Eq. (44), right ordinate) is also largest around the same temporal frequency. Recall that the calculation of the DI is based on the postsynaptic current, not the postsynaptic firing rate. The analytical tuning curves are qualitatively similar to the experimental ones and those obtained from the large scale simulations (see e.g. Saul and Humphrey, 1992, and Fig. 7 in the simulation paper, respectively).

as low pass filters with cut-off frequencies around 8–32 Hz (see e.g. Saul and Humphrey, 1992), however, it is difficult to identify the reason for the loss of DS at high frequencies.

The degree of the selectivity can be expressed by the direction index defined as the normalized difference between the response amplitude for the preferred and non-preferred direction,

$$\mathrm{DI} = \frac{I^1_{right} - I^1_{left}}{I^1_{right} + I^1_{left}}. \tag{44}$$

The right scale of Fig. 6b shows the direction index (DI) as a function of the temporal frequency. Note that the direction index can be greatly enhanced if it is calculated based on the output firing rates rather than on the subthreshold response as done here (cf. Reid et al., 1991; Jagadeesh et al., 1993).

3.5. *Symmetry Breaking for an Unbiased Set of Stimuli*

Next we show that the direction selectivity emerges also in a more natural environment with an unbiased set of stimuli, for instance for drifting gratings with velocity sampled from a Gaussian distribution around 0 deg/s. The idea is that any small deviation from the initial symmetric receptive field initiates a positive feedback loop.

To make this feedback argument somewhat more precise we observe that for a first presentation of a rightward moving stimulus the weight change is $\varepsilon \Delta \bar{G}_{right}$ with some small $\varepsilon > 0$ and $\Delta \bar{G}_{right} \equiv \Delta \bar{G}_d$ given by (33). The corresponding phase shift of the weight distribution is a similar fraction $\epsilon\varphi_x$ of the maximal phase shift φ_x (Eq. (39)) which would be achieved by repeated stimulations from the same direction. This first presentation of a right-drifting grating generates the current $I_{right} \equiv I_d$ from the depressing synapses given by (29). A second grating in the same rightward direction generates a current $I_{right,right}$ which is slightly phase advanced compared to the original one,

$$I_{right,right}(t) = \bar{G}^{\circ}_d\big(f^0_{rel} + s_d f^1_{rel} \cos(\Omega t + \varphi_t + \epsilon\varphi_x)\big).$$

The total postsynaptic current induced by this second grating is obtained from (42) and (43) by replacing φ_x with $\epsilon\varphi_x$. The corresponding weight change is given by (33) with φ_t replaced by $\varphi_t + \epsilon\varphi_x$, and this weight change is larger than the $\varepsilon \Delta \bar{G}_d$ induced by the first. More importantly, for a stimulus moving in the opposite (left) direction, the induced weight change is smaller and cannot annihilate the first. In fact, the postsynaptic current $I^1 = I^1_{right}$ (given by Eq. (36)), which is the main factor determining the weight change $\Delta \bar{G}_{right}$,

Eq. (33), being subject to the synaptic modification, increses after a second stimulus in the same rightward direction to

$$I^1_{right,right} = \sqrt{\left(I^1_d\right)^2 + \left(I^1_{nd}\right)^2 - 2ab\cos(\varphi_t + \epsilon\varphi_x)} > I^1_{right},$$

while for a second stimulus in the opposite (left) direction it decreases to

$$\begin{aligned} I^1_{right,left} &= \sqrt{\left(I^1_d\right)^2 + \left(I^1_{nd}\right)^2 - 2ab\cos(\varphi_t - \epsilon\varphi_x)} < I^1_{right} \\ &= \sqrt{\left(I^1_d\right)^2 + \left(I^1_{nd}\right)^2 - 2ab\cos\varphi_t}. \end{aligned} \tag{45}$$

The relation among the factors of the weight changes results in the same relation among the overall weight changes defined by (33). Note that the phase shift $\epsilon\varphi_x$ induced by the first rightwards drifting grating also affects the argument of the sine in (33). However, the overall amount of LTP and LTD, defined as the integral of (33) over a positive and negative sine half cycle, is proportional to the corresponding factors. Hence, interpreting $\Delta\bar{G}_{right}$ and $\Delta\bar{G}_{right,left}$ in this sense as the overall synaptic LTP or LTD induced by a first rightwards and a subsequent leftwards drifting grating, respectively, we obtain from (45),

$$\Delta\bar{G}_{right} - \Delta\bar{G}_{right,left} > 0,$$

stating that a second grating from the opposite direction cannot invert the synaptic modification initiated by the first and thus can neither invert the induced spatial phase shift. Similarly subsequent alternations of gratings in opposite directions do not annihilate but rather enlarge the initial phase shift towards some asymptotic value φ_x (Fig. 4b). The direction of the first grating therefore introduces a bias which dominates the weight evolution even in the presence of an unbiased set of stimuli.

3.6. *Inseparability of the Spatio-Temporal Receptive Fields*

By definition, a separable spatio-temporal RF can be represented (with respect to a given class of stimuli) as a product of a pure function of space and a pure function of time. Inseparable spatio-temporal RFs are strongly direction selective since only in this case a linearly moving light bar may excite the cell during its whole trajectory through the spatio-temporal RF. To test the spatio-temporal inseparability after learning we drive our model simple cell with a sinusoidally modulated light bar of width σ_B and different retinal positions ξ. Discarding again the nonlinear rectification of the LGN filtering imposed in the simulations we obtain LGN firing rates of the form

$$f_{pre}(x,t) \approx \left(f^0_{pre} + f^1_{pre}\cos(\Omega t)\right)\exp\left(-\frac{(x-\xi)^2}{2\sigma_B^2}\right),$$

with amplitude f^1_{pre} depending on σ_B and ξ. For the sake of simplicity we assume that the light bar and the spatial distribution of the depressing and non-depressing synapses have the same width, $\sigma_B = \sigma_d = \sigma_{nd}$. The currents from the right/left non-depressing surround and from the depressing center are then

$$\begin{aligned} I^{\pm}_{\xi,nd}(t) &= \frac{\bar{G}^{\circ}_{nd}}{2}\left(f^0_{pre} + f^1_{pre}\cos(\Omega t)\right) \\ &\quad\times\exp\left(-\frac{(\xi \mp x_{nd})^2}{2\sigma_b^2}\right), \end{aligned} \tag{46}$$

$$\begin{aligned} I_{\xi,d}(t) &= \frac{\bar{G}^{\circ}_{d}}{2}\left(f^0_{rel} + f^1_{rel}\cos(\Omega t + \varphi_t)\right) \\ &\quad\times\exp\left(-\frac{(\xi + \varphi_x/k)^2}{2\sigma_b^2}\right), \end{aligned} \tag{47}$$

with $\sigma_b = 2\sigma_B/\sqrt{3}$. These expressions are obtained by intergrating (25) and (26), with $\bar{G}^{eff}_d(x)$ replaced by $\bar{G}^{eff}_d(x + \varphi_x/k)$ and coefficients f^0_{rel} and f^1_{rel} given by Eqs. (19) and (20). To further reduce the length of the formulas we neglect the contribution $I^+_{\xi,nd}$ from the left half RF—a situation which is obtained by applying the learning rule to the strength of the non-depressing synapses (see Fig. 4a in the simulation paper). Assuming that the remaining contributions $I^-_{\xi,nd}$ and $I_{\xi,d}$ have roughly the same size (but different phases), the total current takes the form

$$\begin{aligned} I^-_{\xi,nd}(t) + I_{\xi,d}(t) &\approx \cos(\Omega t)\exp\left(-\frac{(\xi+\Delta x)^2}{2\sigma_b^2}\right) \\ &\quad + \cos(\Omega t + \varphi_t)\exp\left(-\frac{\xi^2}{2\sigma_b^2}\right) \\ &= C(\xi)\cos(\Omega t + \Gamma(\xi)), \end{aligned} \tag{48}$$

where $\Delta x = x_{nd} - \varphi_x/k$ denotes the distance between the left RF surround and the RF center. The coefficients

in (48) are obtained through standard trigonometric transforms (see Eq. (53)),

$$\tan \Gamma(\xi) = \frac{\sin \varphi_t}{\cos \varphi_t + \exp\left(-(\xi - \Delta x/2)\Big/\left(\sigma_B^2/\Delta x\right)\right)} \tag{49}$$

and $C(\xi) = \exp(-\xi^2/(2\sigma_B^2))\sqrt{A^2 + B^2}$, with A and B denoting numerator and denominator in (49). According to (48), a sinusoidally modulated light bar positioned at ξ evokes a maximal postsynaptic response at a time $t^{peak} = -\Gamma(\xi)/\Omega$ before its own maximal luminance. The temporal phase advance of the postsynaptic response, $\Gamma(\xi)$ given by Eq. (49), is a sigmoidal function of the bar position ξ. A maximal temporal advance of roughly φ_t/Ω is reached for a bar centered at $\xi = 0$, and a half maximal temporal advance is reached for a bar centered at $\xi = \Delta x/2$, see Fig. 7 a2. The 'slope' of the spatio-temporal RF, $\Delta x/\sigma_B^2 = (x_{nd} - \varphi_x/k)/\sigma_B^2$, is steep if the bar width σ_B is small and/or the induced spatial shift of the RF center, $-\varphi_x/k$, large (note that for the present leftwards shift $-\varphi_x/k$ is positive).

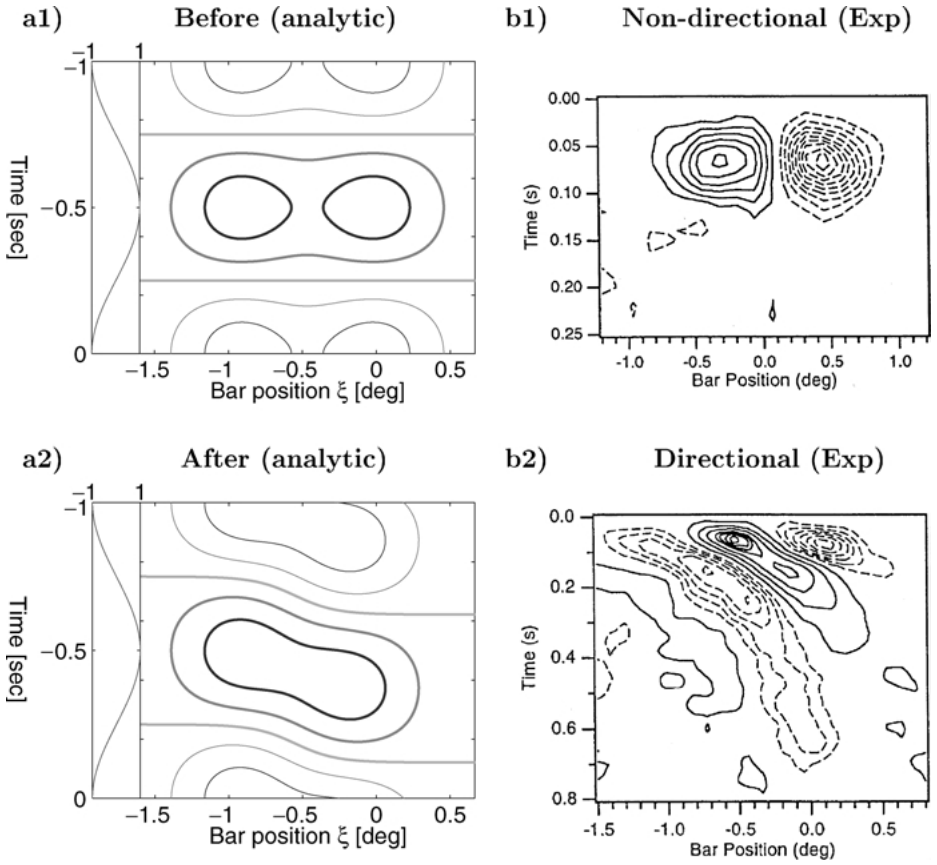

Figure 7. **a:** Spatio-temporal RF of the model simple cell before and after learning. The contour plots show the total postsynaptic current $I(t)$ according to (48) for a bar at retinal position ξ with sinusoidally modulated contrast (traces along the ordinate). Thick lines: excitatory, thin: inhibitory currents. **a1:** Before learning the RF is separable and the cell non-selective ($\varphi_t = \varphi_x = 0$ and $\Gamma(\xi) = 0$ in Eq. (48)). **a2:** After repeated stimulations with drifting gratings the RF becomes inseparable and the cell directional selective because both, the temporal and spatial phase shift emerged ($\varphi_t > 0$ and thus $\Gamma(\xi) > 0$ according to Eq. (49)). If only the temporal shift would develop (like in the 'strobe rearing' scenario, cf. simulation paper, Fig. 9), the two RF clusters in a1 move only along the temporal axes and remain separated in space, making the cell unselective (cf. Humphrey and Saul, 1998, Fig. 6C, for such a 'strobe reared' RF). Same parameter values as in Fig. 3, but $\sigma_B = \sigma_d = \sigma_{nd} = 2/3$ deg, $x_{nd} = 3/4\lambda$. **b:** Spatio-temporal RFs of simple cells in cat area 17, reproduced from Humphrey and Saul (1998). The contour plots represent the simple cell activities in response to bright and dark bars of 40 ms duration, at different locations of the RF. **b1:** Separable RF corresponding to a cell which is not direction selective (DI = 0.08). **b2:** Inseparable RF corresponding to a direction selective cell of a normally reared cat (DI = 0.98, measurement based on the output firing rate).

The response to sinusoidally modulated light bars, Eq. (48), allows us to judge the RF separability, i.e. to test whether the response is a product of a pure function of space and a pure function of time. According to the assumptions in the simulation paper we consider the extended learning scenario where both the synaptic strength, $\bar{G}_d$, and the probability of discharge, P_{dis}, of the depressing synapses are modified by the same learning rule (8). If in the initial state P_{dis} is small, no temporal phase advance is present ($\varphi_t = 0$) and therefore $\Gamma(\xi) \equiv 0$ (formally, $P_{dis} \approx 0$ implies $\varphi_t \approx 0$ in Eq. (21)). As a consequence, the neuronal response (48) becomes a product of a function of space (ξ) and time (t) and the spatio-temporal RF is separable (Fig. 7 a1). As soon as P_{dis} increases during repeated stimulations (see Fig. 4b in the simulation paper), however, a temporal phase advance emerges and the growing component $\Gamma(\xi)$ in Eq. (48) makes the RF inseparable (Fig. 7 a2). Note that the response of the depressing synapses (right oval in Fig. 7 a1) shifts both in time and in space. For comparison, the spatio-temporal RF of an unselective and a selective simple cell is reproduced from Humphrey and Saul (1998) (Fig. 7b).

The joint evolution of the spatial and temporal shift during the learning process is also observed in the large scale simulations (Fig. 9b of the simulation paper, 'normal rearing'), where both phase shifts again have the same size after repeated stimulations. In contrast, in the 'strobe rearing' scenario the directional information is destroyed by the light discontinuities and either no spatial structure could emerge, or the previously acquired spatial structure disappeared (see Fig. 9a and c in the simulation paper, respectively). In terms of our analysis, 'strobe rearing' will leave the two clusters in Fig. 7 a1, well separated in space. Despite the temporal phase advances the RF remains largely separable and the simple cell non-directional.

4. Discussion

We have described long-term modifications of simple cell response properties induced by STDP during exposure to a directionally unbiased stimulus scenario, i.e. to stimuli moving equally often to the left and the right. According to the learning rule, the synaptic strength and the vesicle discharge probability are up- or downregulated, depending on whether the presynaptic activity arises before or after the postsynaptic activity, respectively. The plasticity of the synaptic strength, $\bar{G}$, and the plasticity of the vesicle discharge probability, P_{dis}, leads to the modification of the spatio-temporal RF properties required for DS. Although the temporal resolution of the synaptic modification is below 20 milliseconds, the strongest selectivity develops for drifting gratings with a temporal frequency of roughly 1 Hz (Fig. 6b), i.e. with a peak-to-peak period being almost two order of magnitudes longer than the resolution of the learning rule. Our analysis reveals the following explanations of this and other observations gained from the large scale simulations:

(1) *The temporal frequency tunings of short-term synaptic depression, long-term modifications, and LGN responses are similar*. First, after learning the cell's DS is largest at those frequencies exerting the largest temporal phase advances by means of synaptic depression: with a synaptic recovery time constant $\tau_{rec} = 0.5$ s, a discharge probability $P_{dis} = 0.5$ and a mean LGN firing rate of $f_0 = 40$ spikes/s, an estimate of the optimal temporal frequency is $\Omega/(2\pi) \approx \sqrt{1 + P_{dis} f_{pre}^0 \tau_{rec}}/(2\pi\tau_{rec}) \approx 1$ Hz, see Eq. (22) and Fig. 4a. Second, long-term synaptic modification induces a spatial shift in the RF which is maximal for a stimulus frequency of $\Omega/(2\pi) \approx 1/(2\pi\tau_L) \approx 4$ Hz, provided that the temporal width of the learning function, τ_L, is around 40 ms, see Eq. (37) and Fig. 4b. Third, the LGN firing rate driving the synaptic modifications is itself maximal around a temporal frequency $\Omega/(2\pi) \approx 4.0$ Hz, see Eq. (24) and Fig. 4a. Hence, the temporal phase advance, the spatial RF shift and the LGN responses are largest for a stimulus frequency between 1–4 Hz, and this is two orders of magnitude slower than the temporal width of the learning function (40 ms).

(2) *The match between spatial and temporal phase shifts explain the simple cell DS*. The quantitative agreement of the spatial phase shift, φ_x, and the temporal phase advance, φ_t, explains why a developmental mechanism based on asymmetric STDP and on short-term synaptic depression successfully generates the simple cell DS. In our model, a population of depressing and non-depressing LGN afferents work together in producing DS through their spatial offset and the temporal phase advance of the depressing population. When stimulated in the preferred direction, the two phase shifts add, $\varphi_x + \varphi_t \approx \pi/2$ and, according to the trigonometric summation theorem, the current amplitudes from the depressing and non-depressing

synaptic populations, I_d^1 and I_{nd}^1, respectively, add to $\sqrt{(I_d^1)^2 + (I_{nd}^1)^2}$. When stimulated in the non-preferred direction, however, the two phase shifts cancel, $\varphi_x + \varphi_t \approx 0$, and the currents add to $|I_d^1 - I_{nd}^1|$, see Eq. (43) and Figs. 3b and 5a.

(3) *The temporal frequency determines the absolute value of the RF modification, but not the shape of the RF modification*. The shape and the absolute value of the RF modification are separately determined by the spatial and temporal frequency of the stimulus. More precisely, a drifting grating with spatial and temporal frequencies specified by Ω and k, respectively, induces a change of the synaptic strength, $\Delta\bar{G}(x)$, which is proportional to $-\eta(\Omega)\sin(kx + \gamma)$. Here, $\eta(\Omega)$ is proportional to the Fourier transform of the learning function, and the phase shift γ reflects the interaction of the RF center with the RF surround, see Eq. (33) and Fig. 3b. The expression shows that the shape of the weight change is determined by spatial, and not, as one might expect, by the temporal frequency of the stimulus. What matters for the learning rule, in fact, is not the time difference between the peak of the pre- and post-synaptic activity, but rather the *change* of the presynaptic activity at each position x at the time of the postsynaptic peak activity. Hence, it is the *derivative* of the stimulus which enters in the synaptic modification (as formally expressed in Eq. (58)), and the temporal frequency only appears as an overall scaling factor which can be interpreted as the 'speed' of the synaptic modification. Nevertheless, in a natural stimulation environment with stimuli moving in different directions, this speed determines the steady state value of the spatial RF shift (cf. Fig. 5b in the simulation paper).

(4) *The RF becomes velocity selective when trained with moving bars, but not when trained with moving gratings*. It is worth pointing out that for different types of stimuli, moving narrow bars or moving gratings, the final RF shape is different. RFs formed by moving bars show a stronger velocity selectivity than those formed by drifting gratings. This is because in the case of a moving, infinitely narrow bar the dynamics of the synaptic variables store velocity information at any spatial location, but not in the case of a spatially extended 2-dimensional stimulus. Formally, the synaptic changes at a specific RF position is calculated by the convolution of the learning function with the stimulus, multiplied by the postsynaptic activity (Eq. (31)). The synaptic changes as a function of RF position therefore strongly depends on the type of the stimulus: For a narrow bar, the synaptic changes across the RF reflect the learning function stretched by the stimulus velocity (Eq. (40)). For a moving grating the synaptic changes reflect the derivative of the stimulus at the time of the postsynaptic peak response (Eq. (58)), and the stimulus velocity only enters as a common, non-monotonic factor. The corresponding spatial RF shift is a monotonic function of the stimulus velocity for moving bars, but a non-monotonic function of the temporal frequency for moving gratings (Fig. 4b). As a consequence, we expect a velocity selectivity emerging from the training with narrow bars which is strongest for the same velocity as the cell was trained with. In contrast, such a velocity selectivity, when trained with drifting gratings, is only expected in the low temporal frequency regime where the spatial phase shift is monotonically increasing with the temporal frequency, but not above 8 Hz (Fig. 4b).

(5) *Symmetry breaking in an unbiased stimulus scenario*. DS evolves even when the velocities of the drifting gratings are symmetrically distributed around zero. This is explained by a positive feedback loop which enhances small deviation from the RF symmetry: if a first, rightward drifting grating with response amplitude I_{right}^1 produces a small RF shift $\epsilon\varphi_x$, a second, leftward drifting grating generates a smaller response, $I_{right,left}^1 < I_{right}^1$, because a slight DS already developed for the first direction (Eq. (45)). Since the postsynaptic response goes as a factor into the synaptic modification rule (Eq. (31)) this inequality implies that the RF shift induced by the first, rightward moving stimulus, $\epsilon\varphi_x$, will not be canceled by a second stimulus moving in the opposite direction. In turn, a subsequent stimulus moving in the original rightward direction will further extend the initial phase shift and eventually a macroscopic RF shift φ_x emerges. The robustness of the DS development during exposure to randomly selected stimuli can be further enhanced by nonlinearities in the weight modification. As revealed by the simulation paper, a learning threshold imposed to the postsynaptic activity ensures that the selectivity, once acquired for one direction, remains stable (see point 3 in the Discussion of the simulation paper).

(6) *Interference between RF size and stimulus width.* As discussed in the simulation paper (point 7 of the Discussion), the restriction to a single type of the synaptic modification implies an initial RF structure with depressing synapses in the RF center and non-depressing synapses in the RF surround. Such a RF structure, however, may interfere with the spatial width of the stimulus during the learning process. Due to the spatial periodicity of the drifting gratings, the contribution to the postsynaptic current from the left and right RF surround can be out of phase and, assuming a push-pull mechanism, can cancel each other. They are in phase, however, if the width of the grating corresponds to the width of the RF, $\lambda = 2\pi/k \approx 2x_{nd}$, see Eq. (35) and Fig. 3. More importantly for the learning process, the contribution from the RF center and the surround can be out of phase, and therfore have opposite effects on the modification of RF center, see Fig. 3b, dashed and dotted line. Consequently, when trained with a single grating of different temporal frequencies, the RF size must be adjusted to the spatial frequency of the stimulus, as done in our simulations. In a more general stimulation scenario with randomly distributed spatial frequencies, on the other hand, the development of DS is expected to be dominated by the specific spatial frequency to which the simple cell responds best. In addition, again via positive feedback loop, the perturbation of the RF development by the other, non-optimal stimuli is expected to be eventually suppressed.

(7) *Inseparability of the spatio-temporal RF.* The magnitude of the spatial and temporal phase shift, φ_x and φ_t, determine the degree of the spatio-temporal inseparability of the developing RF, see Fig. 7a2 and Eq. (49), characterizing the temporal phase advance $\Gamma(\xi)$ as a function of the synaptic position ξ. The RF inseparability is a direct expression of the monotonic increase of the temporal phase with position (when discarding one half of the non-depressing surround). To explain the development of a directional RF from an non-directional one, Fig. 7a, we assumed that the synaptic strength, $\bar{G}_d$, and the vesicle release probability, P_{dis}, were both subject to STDP. In fact, due to the joint development of the spatial and temporal phase shift during such a 'normal' rearing scenario, the RF become inseparable and the simple cell direction selective. Deviations from this scenario could explain different misdevelopments. For instance, in a 'strobe' rearing scenario where, in a single model synapse, the information about the stimulus motion is suppressed due to the time slicing by the light flashes, no coherent spatial shift can develop. In this case the asymmetric RF structure either does not develop or disappears when it is already present (cf. simulation paper, Fig. 9). In fact, a spatio-temporal RF which only shows temporal phase shifts without the corresponding spatial phase shift remains to a great extent separable and thus unselective.

In summary, directionally unbiased retinal activity may induce spatially asymmetric synaptic modifications, assuming that the synaptic plasticity itself is temporally asymmetric. The properties of synaptic depression and STDP both support the development of simple cell DS in a physiological regime of temporal frequencies. The developing RF is spatio-temporally inseparable, and its form is differently affected by different stimulus properties: the temporal frequency of the stimulus determines the absolute value, and the spatial frequency determines the shape of the synaptic modifications. This shape is independent of the width of the learning function when stimulated with drifting gratings, but not when stimulated with narrow bars. For a more general discussion and further implications on the learning process see the Discussion in the simulation paper.

Appendix A

A.1. Calculation of the LGN Response

The explicit evaluation of the double integral in Eq. (1) with the spatio-temporal filter functions specified by (2) and (3) yields

$$\int_{-\infty}^{\infty}\int_{-\infty}^{t} d\tilde{x}\, d\tilde{t}\, K(x-\tilde{x})H(t-\tilde{t})\cos(k\tilde{x}-\Omega\tilde{t}) = A_\circ(k,\Omega)\cos(kx-\Omega t+\tilde{\beta})$$

with $A_\circ(k,\Omega) = \sqrt{a^2+b^2-2ab\cos\gamma}$ and some phase shift $\tilde{\beta}$. The constants determining the amplitude are

$$a = 2\frac{e^{-k^2\sigma_c^2/2}-e^{-k^2\sigma_s^2/2}}{1+(\tau_f\Omega)^2},\quad b = \frac{e^{-k^2\sigma_c^2/2}-e^{-k^2\sigma_s^2/2}}{1+(\tau_s\Omega)^2},$$
$$\gamma = 2(\mathrm{atan}(\tau_s\Omega)-\mathrm{atan}(\tau_f\Omega)), \qquad (50)$$

The instantaneous firing rate of the LGN-cell defined by (1) now has the form $f_{pre}(x,t) = \max\{A(C)A_\circ(k,\Omega)\cos(kx-\Omega t), f_{pre}^{back}\}$. Following Chance et al. (1998) the correction factor $A(C)$, taking into account the luminance contrast of the grating, is $A(C) = [172\ln(67C)]^+$ Hz. The contrast is defined as $C = (S_{max}-S_{min})/(S_{max}+S_{min})$, where S_{max} and S_{min} are the maximal and minimal luminance levels of the stimulus. The function $A(C)$ is obtained by fitting the LGN response amplitude with the contrast-frequency curves in Ohzawa et al. (1985), which were recorded with a fixed mean luminance $(S_{max}+S_{min})/2$ (=250 cd/m^{-2}). In both, the simulation and analysis paper we chose a contrast of $C = 0.5$.

Note that the filters K and H slightly differ in two ways from those of Maex and Orban (1996). First, the normalization in the spatial filter is such that for uniform illumination LGN-responses are small. This is based on the fact that for wide gratings ($k \to 0$) the LGN and simple cells responses are small (Saul and Humphrey, 1990, 1992). Second, the temporal filter has a stronger excitatory component in order to obtain high enough LGN firing rates for slow temporal frequencies.

The above double integral is calculated by means of the two formulas

$$\frac{1}{\tau^2}\int_{-\infty}^{t} d\tilde{t}(t-\tilde{t})e^{-\frac{t-\tilde{t}}{\tau}}\cos(k\tilde{x}-\Omega\tilde{t}) = \frac{1}{1+(\tau\Omega)^2}\cos(-k\tilde{x}+\Omega t+2\arctan\tau\Omega), \quad (51)$$

$$\frac{1}{\sqrt{2\pi}\sigma}\int_{-\infty}^{\infty} d\tilde{x}\exp\left(-\frac{(x-\tilde{x})^2}{2\sigma^2}\right)\cos(-k\tilde{x}+\psi) = \exp\left(-\frac{k^2\sigma^2}{2}\right)\cos(kx-\psi). \quad (52)$$

In addition to these integrals we used the trigonometric transform

$$a\cos\alpha - b\cos(\alpha-\gamma) = c\cos(\alpha-\beta), \quad (53)$$

where $c = \sqrt{a^2+b^2-2ab\cos\gamma}$ and $\tan\beta = b\sin\gamma/(b\cos\gamma - a)$.

A.2. Estimate of the Temporal Phase Advance

To get the first order Fourier approximation of P_v in response to a sinusoidal stimulation $f(t) = f^0 + f^1\cos(\Omega t)$ we make the ansatz $P_v(t) \approx P_v^0 + P_v^1\cos(\Omega t+\phi)$, thereby neglecting higher order terms. Inserting this into (9) and decomposing the product of cosines into a sum of cosines we get

$$\Omega P_v^1\sin(\Omega t+\phi) \approx -\frac{1}{\tau} + P_v^0 a + P_v^1 a\cos(\Omega t+\phi) + P_v^0 b\cos(\Omega t) + P_v^1 b\cos(\phi)/2,$$

with $a = 1/\tau + P_{dis}f^0$, $b = P_{dis}f^1$, $\tau = \tau_{rec}$, and where we neglected the second order term $-P_v^1 b/2\cos(2\Omega t+\phi)$ on the right-hand side. Transforming the cosines of the sums into products of sines and cosines, we obtain the following coefficients for the zero order term, the $\sin(\Omega t)$-term, and the $\cos(\Omega t)$-term, respectively,

$$0 \approx -1/\tau + P_v^0 a + P_v^1 b\cos(\phi)/2, \quad (54)$$

$$\Omega\cos\phi \approx -a\sin\phi, \quad (55)$$

$$\Omega P_v^1\sin\phi \approx P_v^1 a\cos\phi + P_v^0 b. \quad (56)$$

From (55) we directly get the phase advance ϕ, Eq. (15), and we also deduce that $\sin\phi = \Omega/F$ and $\cos\phi = -\Omega\tau/F$, with $F^2 = a^2+\Omega^2$. Inserting this into (56) we get (14), and together with (54) we obtain (13).

To approximate the Fourier terms (18) for the synaptic release rate we expand (17) by a trigonometric transform into

$$f_{rel}(t) \approx P_{dis}\left(P_v^0 f_{pre}^0 + \frac{P_v^1 f_{pre}^1}{2}\cos\phi + P_v^0 f_{pre}^1\cos\Omega t + P_v^1 f_{pre}^0\cos(\Omega t+\phi)\right),$$

where we dropped the second order term $\frac{P_v^1 f_{pre}^1}{2}\cos(2\Omega t+\phi)$ in the parentheses. According to this approximation the phase advance of f_{rel} is a weighted sum between the phases 0 and ϕ, with a bias towards 0 due to the discarded term. Substituting the approximation for ϕ and using formula (53) we obtain the spatial phase advance and the zero- and first order Fourier coefficients of the synaptic release rate $f_{rel}(t)$, Eqs. (19)–(21).

A.3. Estimate of the Spatial Phase Advance

The total currents from the non-depressing and depressing synapses, I_{nd}/d (Eqs. (28) and (29)), are obtained by applying formula (52) to the integrals (25) and (26).

To calculate (31) we rewrite the weight modification in a Hebbian form as a product of a pre- and postsynaptic term,

$$\Delta\bar{G}_d(x) = \frac{1}{T}\int_0^T dt P(x,t)I(t) \tag{57}$$

The presynaptic term $P(x,t)$ is obtained by convolving the instantaneous release rate (27) with the learning function (8),

$$\begin{aligned} &P(x,t)\\ &\quad= \int_{-\infty}^{\infty} d\tilde{t}\, L(\tilde{t}) f_{rel}(x,\tilde{t}+t)\\ &\quad= -\frac{\tau_L}{\sqrt{2\pi}}\int_{-\infty}^{\infty} d\tilde{t}\exp\left(-\frac{\tilde{t}^2}{2\tau_L^2}\right)\frac{d}{dt} f_{rel}(x,\tilde{t}+t)\\ &\quad= -f^1_{rel}\eta(\Omega)\sin(kx-\varphi_t-\Omega t), \end{aligned} \tag{58}$$

where $\eta(\Omega) = \tau_L^2\Omega\exp(-\tau_L^2\Omega^2/2)$. In this calculation we first applied the transform

$$\begin{aligned} &\frac{1}{\tau^2}\int_{-\infty}^{\infty}\tilde{t}\exp\left(-\frac{\tilde{t}^2}{2\tau^2}\right) f(\tilde{t}+t)\,d\tilde{t}\\ &\quad= \int_{-\infty}^{\infty}\exp\left(-\frac{\tilde{t}^2}{2\tau^2}\right)\frac{d}{dt} f(\tilde{t}+t)\,d\tilde{t}, \end{aligned}$$

obtained by partial integration, and then applied another time formula (52). Summing up the synaptic currents from the RF center and the surround, Eqs. (28) and (29), one obtains

$$\begin{aligned} I(t) &= I_d(t) + I^-_{nd}(t) + I^+_{nd}(t)\\ &= I^0 + I^1_d\cos(\varphi_t+\Omega t) - I^1_{nd}\cos(\Omega t) \end{aligned}$$

with coefficients I^1_d and I^1_{nd} given by (35). By means of

$$\frac{1}{T}\int_0^T dt\sin(a-\Omega t)\cos(b-\Omega t) = \frac{1}{2}\sin(a-b)$$

the integral (57) now evaluates to (32) and the weight change $\Delta\bar{G}_d(x)$ given in the form (33) is obtained by standard trigonometric transforms, see Eq. (53).

To calculate the change in the synaptic strength induced by an infinitely narrow bar moving across the RF we evaluate the inner integral in (31) while dropping the averaging over the period T. For the synaptic release rate $f_{rel}(x,t) = P_{dis}f^0_{pre}\delta(vt-x)$ and the postsynaptic current $I(t) = I_d(t) = P_{dis}f^0_{pre}\bar{G}^{eff}_d(vt)$ induced by the depressing synapses, cf. Eq. (6) and (26), we get

$$\begin{aligned} \Delta\bar{G}_d(x) = \frac{P_{dis}f^1_{pre}\bar{G}^\circ_d}{\sqrt{2\pi}}&\frac{-xv\tau_L^2}{\left((v\tau_L)^2+\sigma_d^2\right)^{\frac{3}{2}}}\\ &\times\exp\left(\frac{-x^2}{2\left((v\tau_L)^2+\sigma_d^2\right)}\right). \end{aligned} \tag{59}$$

If we also consider the contribution of the postsynaptic currents $I^\pm_{nd}$ to $\Delta\bar{G}_d(x)$ we have to add in (59) another two terms obtained by replacing x with $x\pm x_{nd}$ and σ_d with σ_{nd}. To evaluate the integral in (31) we made use of the formula

$$\begin{aligned} &\int_{-\infty}^{\infty} t\exp\left(-\frac{t^2}{2\tau_L^2}\right)\exp\left(-\frac{(\tau-t)^2}{2\sigma^2}\right)dt\\ &\quad= \frac{\sqrt{2\pi}\tau\sigma\tau_L^3}{\left(\tau_L^2+\sigma^2\right)^{\frac{3}{2}}}\exp\left(\frac{-\tau^2}{2\left(\tau_L^2+\sigma^2\right)}\right). \end{aligned} \tag{60}$$

Finally, to find the location $x^{peak}_{\Delta G}$ of the maximal weight change $\Delta\bar{G}^{eff}_d(x)$ given by (38) we look for the first negative solution of $\frac{d}{dx}\Delta\bar{G}^{eff}_d(x) = 0$. Calculating this derivative, we obtain after some transforms

$$x^{peak}_{\Delta G}\tan\left(kx^{peak}_{\Delta G}-\gamma\right) = k\sigma_d. \tag{61}$$

Since $x^{peak}_{\Delta G}$ is expected to be in the interval $[0,\frac{\pi}{2}]$ we approximate the tangens by a hyperbole,

$$\tan\left(kx^{peak}_{\Delta G}-\gamma\right) \approx -\frac{1}{\frac{\pi}{2}+kx^{peak}_{\Delta G}-\gamma}.$$

Inserting into (61) and solving for $x^{peak}_{\Delta G}$ leads to the estimate (39) of the spatial phase advance φ_x.

Acknowledgments

This study was supported by the Swiss National Science Foundation (grant 21-57076.99) and the Silva Casa foundation. We would like to thank Stefano Fusi for helpful discussions and David Thurbon for proof reading.

References

Albrecht D, Farrar S, Hamilton, D (1984) Spatial contrast adaptation characteristics of neurones recorded in the cat's visual cortex. J. Physiol. (London) 347: 713–739.

Bi G, Poo M (2001) Synaptic modification by correlated activity: Hebb's postulate revisited. Annu. Rev. Neurosci. 24: 139–166.

Buchs N, Senn W (2002) Spike-based synaptic plasticity and the emergence of direction selective simple cells: Simulations results. J. Computational Neuroscience 13(3): 167–186.

Carandini M, Heeger D, Movshon J (1997) Linearity and normalization in simple cells of the macaque primary visual cortex. Journal of Neuroscience 17(21): 8621–8644.

Carandini M, Heeger D, Senn W (2002) A synaptic explanation of suppression in visual cortex. J. Neuroscience 22(22): 10053–10065.

Chance F, Nelson S, Abbott L (1998) Synaptic depression and the temporal response characteristics of V1 cells. J. Neuroscience 18(12): 4785–4799.

Freeman T, Durand S, Kiper D, Carandini M (2002) Suppression without inhibition in visual cortex. Neuron 35: 759–771.

Fu YX, Djupsund K, Gao H, Hayolen B, Shen K, Dan Y (2002) Temporal specifity in the cortical plasticity of visual space representation. Science 296(5575): 1999–2003.

Hubel D, Wiesel T (1962) Receptive fields, binocular interaction and functional architecture in the cat's visuals cortex. J. Physiol. (London) 160: 106–154.

Humphrey A, Saul A (1998) Strobe rearing reduces direction selectivity in area 17 by altering spatiotemporal receptive-field structure. J. Neuroscience 80: 2991–3004.

Jagadeesh B, Wheat H, Ferster D (1993) Linearity of summation of synaptic potentials underlying direction selectivity in simple cells of the cat visual cortex. Science 262: 1901–1904.

Maex R, Orban G (1996) Model circuit of spiking neurons generating directional selectivity in simple cells. J. Neurophysiol 75: 1515–1545.

Markram H, Tsodyks M (1996) Redistribution of synaptic efficacy between neocortical pyramidal neurons. Nature 382: 807–810.

Morrone M, Burr D, Maffei L (1982) Functional implications of cross-orientation inhibition of cortical visual cells. I. Neurophysiological evidence. Proc. R. Soc. Lon. B 216: 335–354.

Ohzawa I, Sclar G, Freeman R (1985) Contrast gain control in the cat's visual system. J. Neurophysiol. 54: 651–667.

Reid R, Soodak R, Shapley R (1987) Linear mechanisms of directional selectivity in simple cells of cat striate cortex. Proc. Natl. Acad. Sci. USA 84(23): 8740–8744.

Reid R, Soodak R, Shapley R (1991) Directional selectivity and spatiotemporal structure of receptive fields of simple cells in cat striate cortex. J. Neurophysiol. 66(2): 505–529.

Saul A, Humphrey A (1990) Spatial and temporal response properties of lagged and nonlagged cells in cat lateral geniculate nucleus. J. Neurophysiol. 64: 206–224.

Saul A, Humphrey A (1992) Temporal frequency tuning of direction selectivity in cat visual cortex. Vis. Neurosci. 8: 365–372.

Senn W, Tsodyks M, Markram H (2001) An algorithm for modifying neurotransmitter release probability based on pre- and postsynaptic spike timing. Neural Computation 13(1): 35–68.

Senn W (2002) Beyond spike-timing: The role of nonlinear synaptic plasticity and unreliable synapses. Biol. Cybernetics 87: 344–355.

Shapley R (1996) Linearity and non-linearity in cortical receptive field. Ciba Found Symp 184: 71–87.

Stratford K, Tarczy-Hornoch K, Martin K, Baninster N, Jack J (1996) Excitatory synaptic inputs to spiny stellate cells in cat visual cortex. Nature 382: 258–261.

Yao H, Dan Y (2001) Stimulus timing-dependent plasticity in cortical processing of orientation. Neuron 32: 315–323.